

Quantifying Runoff Generation Mechanisms in the Grand River Watershed and their Relationship to Nutrient Concentrations using MCE

Claire Haar, Nicolas Perciballi, Nicholas Puopolo

GEOG*4480

Ben DeVries

April 16, 2021

Contents

Abstract.....	3
1. Introduction	3
2. Study Area.....	4
3. Methods and Data	5
3.2 Individual Environmental Criteria	6
3.2.1 NDVI	6
3.2.2 Land Use.....	8
3.2.3 Hydrologic Soil Groups.....	10
3.2.4 Topographic Wetness Index (TWI).....	11
3.3 Factor Weightings	12
3.4 MCE Algorithm	13
3.5 Linear Regression Analysis	14
4. Results.....	16
4.1 Runoff Generation Indexes	16
4.2 Relationships Between Normalized Runoff Generation Indexes and Average Phosphorus Concentrations at the Sub-Watershed Scale	18
5. Discussion.....	19
6. Conclusion.....	20
References	21

Abstract

Currently, there is a gap in our understanding of how to quantify hydrologically active areas (HAAs) and how they relate to nutrient loadings at the watershed scale (Ali *et al.*, 2017; Sen *et al.*, 2008). This study provides a simple modelling approach quantifying the potential for saturation-excess (SOF) and infiltration-excess overland flow (IOF), and assesses their relationships with phosphorus concentrations in the Grand River watershed. The potential for HAAs was quantified using three criteria for each runoff generation mechanisms (RGM) in a multi-criteria evaluation (MCE). The criteria included: a normalized difference vegetation index (NDVI) computed using multiple 30 m resolution LANDSAT 8 images captured in 2015; land use data compiled using a 15 m resolution raster retrieved from the SOLRIS (2015) dataset; hydrological soil group vector dataset with 1:10,000 scale, retrieved from the Soil Survey Complex dataset compiled by the Ontario government; and a topographic wetness index computed using a 1 m resolution digital terrain model, retrieved from the Government of Canada's High-Resolution Digital Elevation Model (HRDEM). A normalized RGM index score was calculated for each sub-watershed in the study area for each RGM. These scores were compared with monitored phosphorus concentrations using a linear regression to evaluate potential relationships. Results from the regression indicated that IOF had an $R^2 = 0.312$, while SOF had an $R^2 = 0.087$, highlighting a stronger correlation between IOF and nutrient concentrations than SOF. The results provide a basis for new approaches to restoration techniques, whereby targeting areas more conducive to IOF may yield more effective results in controlling the transport of phosphorus from land surface to stream. Ideally, this will be used in conjunction with known high nutrient loading zones to identify the most important target areas for mitigation.

1. Introduction

Our understanding of the linkages between nutrient source zones, surface water pathways, and channel water quality remains incomplete (Ali & Creed, 2017; Calhoun *et al.*, 2017; Wu & Lane, 2017). Hydrological characteristics of the landscape play an important role in the conversion of rainfall to runoff, and the presence of surface flow pathways is an important factor controlling transport of sediment and nutrients across landscapes (Ali & Creed, 2017; Heathwaite *et al.*, 2005; Sen *et al.*, 2010; Outram *et al.*, 2016). The development of a simplistic and computationally manageable model to quantify surface flow pathways is a necessary first step to assess possible impacts on nutrient loadings.

Phosphorus (P), a nutrient found in high concentrations in agricultural catchments, predominantly binds to sediments and is transported to stream networks after becoming entrained in surface runoff (Molder *et al.*, 2015; Sen *et al.*, 2009). The mechanisms which allow for surface runoff generation can be categorized as saturation-excess or infiltration-excess overland flow (Ali *et al.*, 2017). Saturation-excess overland flow (SOF) occurs when the soil column becomes completely saturated with water, hindering any additional infiltration and causing additional water to flow along the surface (Hoang *et al.*, 2017; Srinivasan *et al.*, 2002).

Alternatively, infiltration excess overland flow (IOF), also referred to as Hortonian overland flow, occurs when the precipitation rate exceeds the soil infiltration rate, causing runoff generation before the soil column becomes saturated (Reli *et al.*, 2016; Srinivasan *et al.*, 2002). SOF and IOF can vary spatially and temporally based on land-use, topography, and climate, which has allowed scientists to identify areas within a landscape where these mechanisms are likely to occur (Gburek & Sharpley, 1998; Srinivasan *et al.*, 2001, 2002). These runoff generating areas, deemed as hydrologically active areas (HAAs), have been shown to contribute disproportionately to P transport and the hydrological response of watersheds (Ali *et al.*, 2017; Sen *et al.*, 2008; Zollweg *et al.*, 1995). A study conducted by Zollweg *et al.* (1995) found that a 1% change of land-use in HAAs reduced the transport of dissolved P by 24%, highlighting the importance runoff can have when transporting nutrients throughout a catchment.

Although our current understanding of watershed connectivity and the delivery of nutrients from landscapes to channel networks is limited, few studies have sought to quantify runoff generating areas (Ali & Creed, 2017; Calhoun *et al.*, 2017; Wu & Lane, 2017). GIS approaches to hydrology and runoff modelling provide a way to analyze hydrological processes spatially, which is useful for implementing targeted mitigation efforts and accurately quantifying HAAs in specific regions. This study will use a multi criteria evaluation (MCE) to quantify the spatial variability of HAAs based on two runoff generation mechanisms (RGMs), SOF and IOF. An MCE will not definitively quantify the presence of runoff flow pathways; rather, it will predict where HAAs could occur based on environmental conditions that facilitate specific RGMs. Through applying different environmental criteria in an MCE, we can consider multiple factors and identify if a distinct type of runoff is likely to occur through the creation of runoff generation indexes. These indexes may be used to quantify the relative degree of hydrological activity within a watershed for each RGM. Assuming HAAs can be quantified on a landscape, the correlation between P concentrations and surface runoff potential can be assessed.

Several studies have suggested runoff generation is spatially variable, and that HAAs and runoff pathways are important for nutrient transport (Ali *et al.*, 2017; Gburek & Sharpley, 1998; Sen *et al.*, 2010). Therefore, the objectives of this study are to:

1. Identify relevant environmental criteria that facilitate RGMs (IOF and SOF) and prepare datasets for MCE models.
2. Generate RGM indexes (MCE model outputs) that quantify potential HAAs.
3. Assess the relationship between RGM indexes and phosphorus concentrations in associated stream networks.
4. Assess the strengths and limitations of the MCE model approach for quantifying HAAs.

2. Study Area

The location for the study is the Grand River Watershed (GRW) located in southern Ontario, Canada (Figure 1). This is the largest Canadian watershed (6,800 km²) which drains into Lake Erie, the most nutrient polluted of all the great lakes (GRCA, 2020; ECCC,

2018). Historically, agricultural land use practices which dominate the watershed have led to high levels of nutrients becoming mobilized during runoff events, leading to large algal blooms and other water quality concerns in receiving waters (Watson *et al.*, 2016). Therefore, examining the extent of HAAs for various RGMs in the GRW may allow us to determine the possible nutrient transport pathways into the stream network and ultimately Lake Erie.

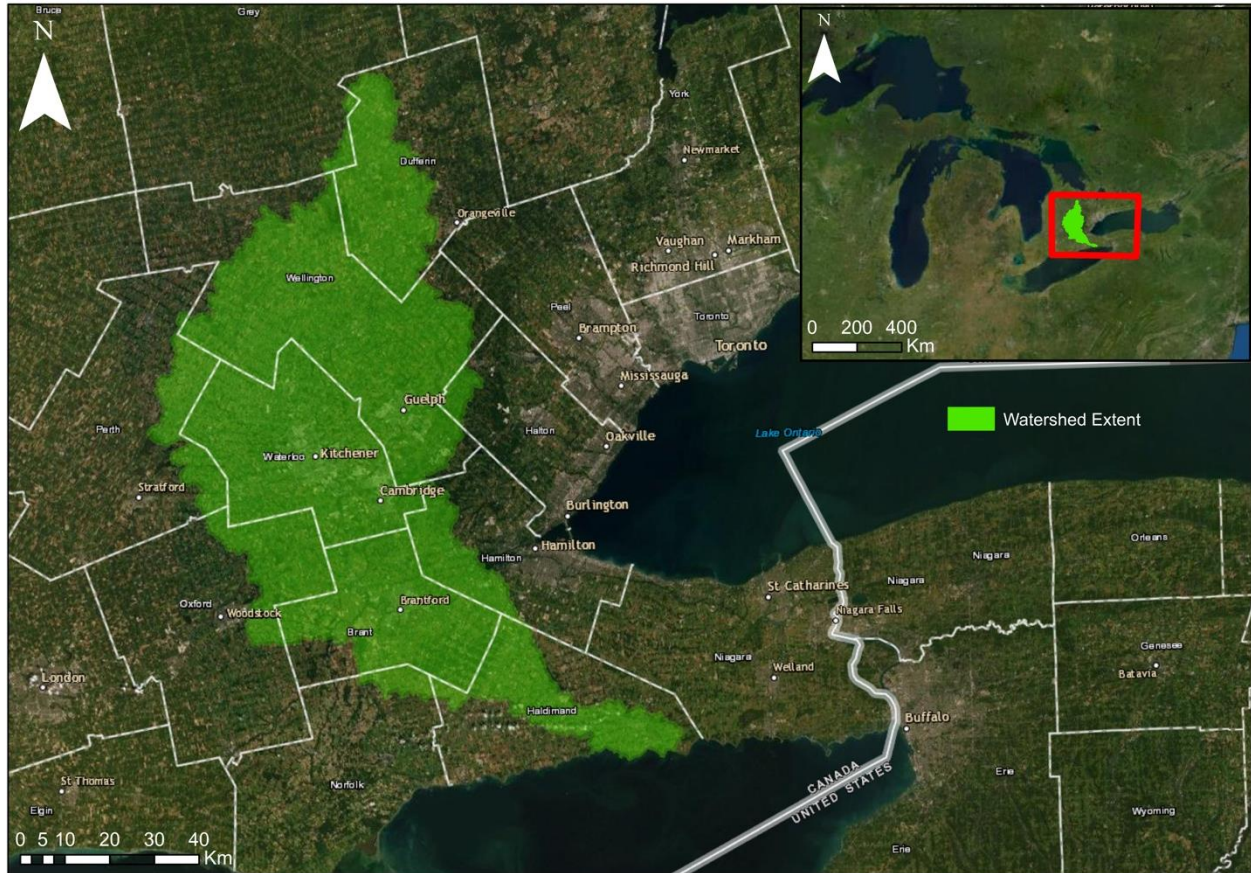


Figure 1: The Grand River Watershed, as seen from a larger scale to a smaller scale. The Watershed boundary was exported from Grand River Information Network (2018). The base-map was created using ArcGIS® software and imagery provided by Esri.

3. Methods and Data

To produce viable, yet effective MCE models, both RGMs (SOF and IOF) need to be quantified separately, as evaluating them simultaneously has shown limitations in accuracy (Liu *et al.*, 2020). The SOF mechanism typically occurs in low-lying topographic regions, and areas near streams and gullies. Alternatively, the IOF mechanism typically occurs on relatively impermeable surfaces such as urban roads and dry or compacted agricultural fields. Since there are variable areas throughout the watershed that facilitate each RGM, creating two MCEs to look at SOF and IOF independently will ensure both runoff types are being accurately quantified within the watershed.

Three factors were chosen for each runoff generation type and identified through expert consultation and reviews of relevant literature (Table 1). The included criteria represent only static environmental variables, rather than dynamic variables such as storm characteristics and antecedent moisture conditions. There exists a large knowledge gap in how storm

characteristics and catchment moisture control P flux, thus making predictions about nutrient concentrations based on precipitation events difficult (Davis *et al.*, 2014). Therefore, we chose to include proxies for only the most important and well-researched factors controlling the proportion of precipitation that is converted to runoff (Table 1). To facilitate accurate processing and support the robust computation and interaction of data layers, all layers were generated in raster format with 5 m cell resolution and reprojected to NAD83 UTM Zone 17 N. The datasets were clipped to the extent of the GRW, and all layers were standardized to a common scale using a basic linear stretch, shown in Equation 1 as:

$$EQUATION\ 1: \quad x'_{ij} = Range \left(\frac{x_{ij} - x_{min}}{x_{max} - x_{min}} \right)$$

where x'_{ij} is the standardized score for a given cell in the output raster, range is the standardized scale (0-1), x_{ij} is the value for a given cell in the input raster, x_{min} and x_{max} are the minimum and maximum cell values for the input raster (Bonnycastle *et al.*, 2017).

Table 1: Criteria used for SOF and IOF MCE models.

SOF	IOF
1. Topographic Wetness Index	1. Hydrologic Soil Groups
2. Normalized Difference Vegetation Index (NDVI)	2. Normalized Difference Vegetation Index (NDVI)
3. Land-use Data	3. Land-use Data

3.2 Individual Environmental Criteria

3.2.1 NDVI

LANDSAT 8 images, obtained from USGS (2020) with a filter date of April 1, 2015 – November 1, 2015, were used to generate a median normalized difference vegetation index (NDVI). The NDVI is the result of combining the spectral signatures from the red (RED) and near infrared (NIR) bands using Equation 2 and provides an accurate indication of the health and density of vegetation cover across a landscape (Brown, n.d.). Note, to produce accurate index results, cloud cover and cloud shadows were masked out of the image prior to calculation. NDVI was chosen as a criterion because vegetation cover is an important factor governing the conversion of rainfall to runoff (Liu *et al.*, 2020). As vegetation health and density increases, the likelihood of interception, evapotranspiration, and root water uptake also increases (Liu *et al.*, 2020). This reduces the rate and volume of water that reaches the soil layer, thus limiting runoff generation. Since the NDVI quantifies vegetation broadly into discrete classes (Table 2), generalizations about the processes controlling runoff generation were made to reclassify the data. A generalized ranking for the likelihood of runoff generation was assigned to the three vegetation classes (Table 3), based on the findings from Zimmermann, Elsenbeer, and De Moraes (2006). As land-use is considering all land-cover types, by including the NDVI separately we isolate the impacts from vegetation from the impacts of all land covers.

$$\text{EQUATION 2: } NDVI = (NIR - RED)/(NIR + RED)$$

Table 2: Reclassification of the NDVI values to three classes based on the scheme outlined by Brown (n.d.).

Vegetation Classes	Description	NDVI Value
0 - Non-Vegetation	Barren, built-up areas, and road networks.	-1 to 0.199
1 - Low Vegetation	Sparse Vegetation	0.200 to 0.500
2 - High Vegetation	Dense Vegetation	0.501 to 1

Table 3: Specific NDVI classifications for both the SOF and IOF, derived from the findings of Zimmermann, Elsenbeer, and De Moraes (2006).

Vegetation Class	Runoff Score
0 - Non-Vegetation	2 - Highly Likely
1 - Low Vegetation	1 - Possible
2 - High Vegetation	0 - Unlikely

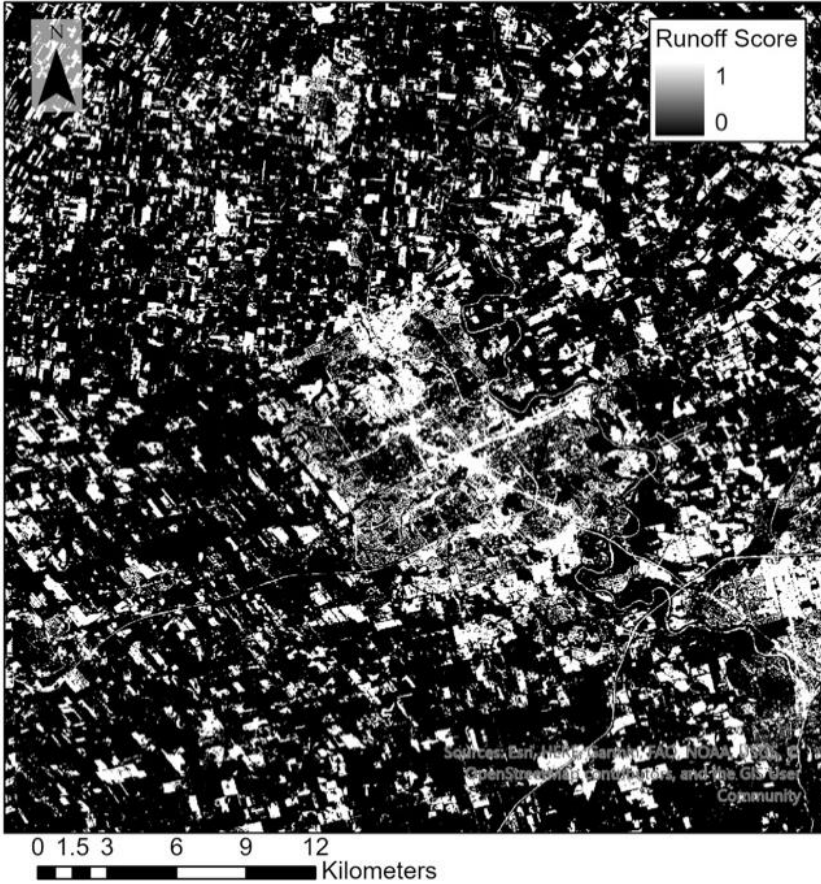


Figure 2: Map of the runoff index for NDVI based on the suitability classification in Table 4. White (value = 1) regions of the map depict areas where vegetation characteristics are conducive for runoff generation, and black (value = 0) represents areas where runoff generation is highly unlikely.

3.2.2 Land Use

A 15 m resolution land-use raster was retrieved from the SOLRIS (2015) dataset. Certain land-use types have known implications on hydrological responses (Endreny, 2005). However, only broad assumptions can be made about how certain land classes will impact runoff generation (Niehoff, Fritsch, & Bronstert, 2002). Because land-use only provides broad classifications based on generalized above-surface features and does not account for specific topographical, vegetation, or soil characteristics that can influence runoff generation, it was allotted the lowest weighting. However, land-use data fills gaps in the NDVI data relating to specific vegetation classes. While NDVI does not discretely classify vegetation types, land-use addresses these vegetation differences (crops, grasslands, forests, etc.). The original dataset was reclassified from thirty-two discrete classes to eleven based on similar land-use characteristics (Table 4). This was then reclassified into 4 key classes which represent how conducive each land use type is for each RGM (Table 5).

Table 4: Reclassified land-use data, based on the similarities in land-use type.

Reclassified Data	
Land-Use Class	New Class ID
Beach/Sand Dunes	0
Exposed Bedrock	1
Grasslands	2
Forests	3
Wetlands	4
Open Water	5
Agriculture	6
Urban	7
Extraction: Gravel	8
Extraction: Peat	9
Other	10

Table 5: Land-use classes created for both the SOF and IOF, derived from the findings of: Endreny, 2005; Lyon, McHale, Walter, & Steenhuis, 2006; and Niehoff, Fritsch, & Bronstert, 2002.

Newly Reclassified ID	Categories Reclassified Based on Runoff Generation Likelihood	
Likelihood Ranking	Likelihood of IOF	Likelihood of SOF
0 - Very Unlikely	Beach/Sand Dunes; Wetlands; Extraction; Gravel	Beach/Sand Dunes; Exposed Bedrock; Forests; Extraction: Gravel
1 - Unlikely	Forests	Agriculture; Urban; Extraction: Peat
2 - Likely	Grasslands; Agriculture; Extraction: Peat; Other	Grasslands; Other
3 - Highly Likely	Exposed Bedrock; Urban; Open Water	Wetlands; Open Water

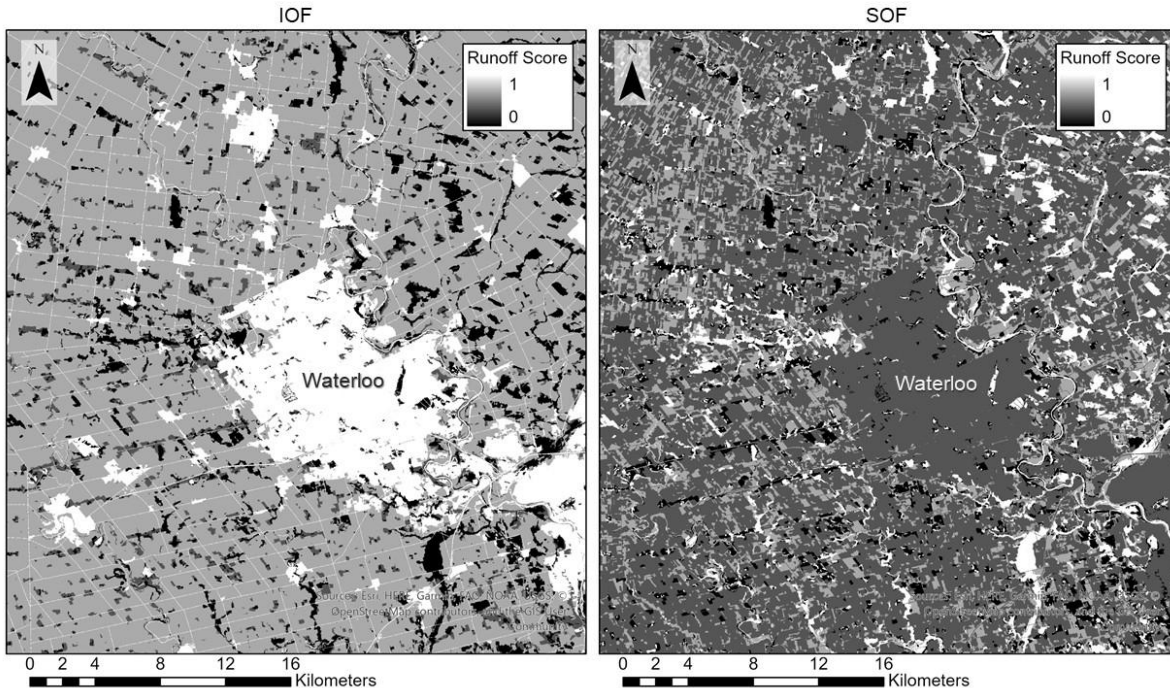


Figure 3: Map of the runoff indexes for land-use types based on the suitability classification in Table 6. The left and right maps depict the resulting land use suitability maps for IOF and SOF respectively. White (value = 1) regions of the map depict areas where land-use characteristics are conducive for runoff generation, and black (value = 0) represents areas where runoff generation is highly unlikely.

3.2.3 Hydrologic Soil Groups

Hydrologic Soil Groups were retrieved from the Soil Survey Complex dataset compiled by the Ontario government. It is composed of vector polygons and has a 1:10,000 scale. This dataset is classified based on the infiltrability of the soil, which is the most important factor determining the capacity for IOF (Helalia, 1993). More porous soils like gravels and sands are much easier for water to infiltrate and therefore have a lower capacity for IOF runoff generation (Reli *et al.*, 2016). Finer soils like silts and clays have smaller pores, slowing the rate at which water can infiltrate and are therefore more conducive to IOF (Reli *et al.*, 2016). Soils were classified based on their capacity for infiltration and runoff generation potential as described in Chisholm *et al.* (1984) (Table 6).

Table 6: Soil group classes based on capacity for IOF runoff generation.

Soil Group	Likelihood of IOF
Very High Porosity	1
High Porosity	2
Low Porosity	3
Very Low Porosity	4
Impervious Surfaces	5

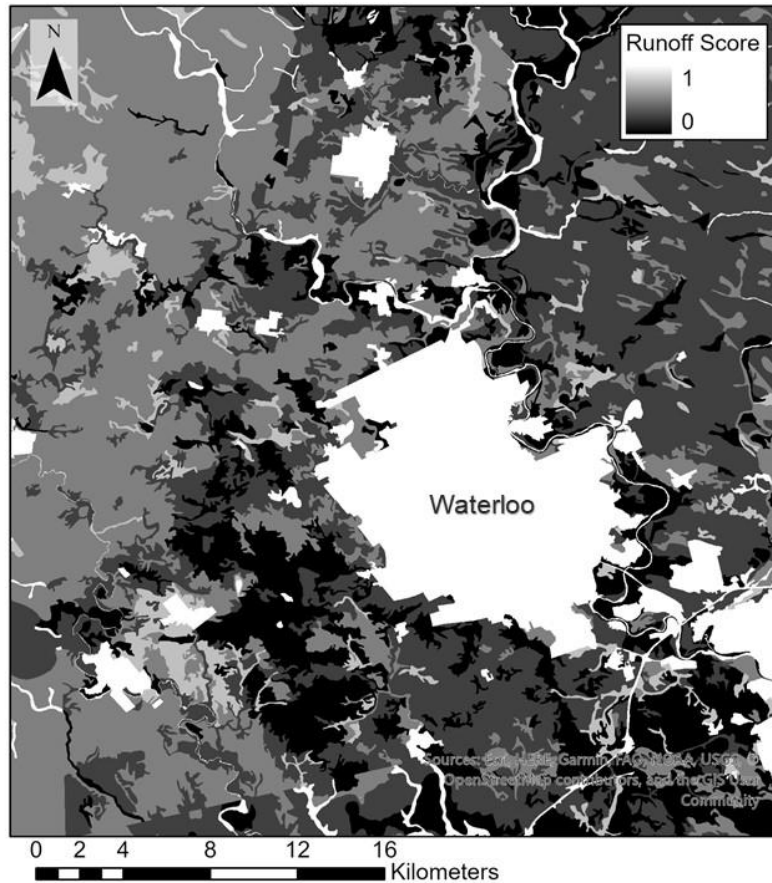


Figure 4: Map of the runoff index for hydrological soil characteristics based on the suitability classification in Table 7. White (value = 1) regions of the map depict areas where soil characteristics are conducive for IOF runoff generation, and black (value = 0) represents areas where the occurrence of IOF is highly unlikely.

3.2.4 Topographic Wetness Index (TWI)

The most important factor governing the generation of SOF is topography (Hoang *et al.*, 2017). Topographic wetness index (TWI) is one of the most used hydrologically based topographic indexes and is defined as follows:

$$\text{EQUATION 3: } TWI = \ln\left(\frac{\alpha}{\tan\beta}\right)$$

where α is the Specific Catchment Area (SCA) (also known as flow accumulation) and β is the slope angle (Małgorzata *et al.*, 2018; Mattivi *et al.*, 2019). Areas prone to water accumulation will be linked to high TWI values, and are more likely to generate SOF. A 1 m resolution digital terrain model (DTM) was retrieved from the High-Resolution Digital Elevation Model (HRDEM) dataset compiled using LiDAR data by the Government of Canada (Government of Canada, 2020). Depression filling is required to prepare DTM data sets for hydrological analyses (Lindsay, 2020). The *DepressionBreachingLeastCost* tool available from Whitebox Tools was used because it offers a lower-impact alternative to depression filling to remove topographic depressions (Lindsay, 2020). The breached DTM was then used to calculate flow direction and slope. Using the spatial analyst work package in ArcGIS, flow direction (FD) was calculated using

the *Flow Direction* tool and the *D-inf* flow algorithm, and slope was calculated in degrees using the *Slope* tool. The FD layer was subsequently used as an input to compute flow accumulation (SCA) using the *Flow Accumulation* tool available in ArcGIS.



Figure 5: Map of the runoff index for the topographic wetness index (TWI), whereby higher TWI values correspond to areas of water accumulation (a.k.a., landscape drainage or surface flow pathways). White (value = 1) regions of the map depict areas where the topography of the landscape is conducive for SOF runoff generation, and black (value = 0) represents areas where the occurrence of SOF is highly unlikely.

3.3 Factor Weightings

Since some factors are more important for generating runoff than others, it is necessary to assign weights to each criterion (Bonnycastle, *et al.*, 2017). Pairwise comparison matrixes (PCM) were used to establish factor weights for each assessment (IOF and SOF). This is a common method used for MCEs, whereby factor layers are compared two at a time, and the relative importance of one factor over another is assigned using a hedonic scale (Bonnycastle, *et al.*, 2017; Saaty, 1977). Relevant literature and expert opinions were used to ascertain the relative importance of each criterion, and scores were assigned based on interpretations of the findings from interviews and literature review. An example of the PCM for IOF depicts how initial weights are assigned (pairwise ranks) and related to the individual and total weights (Table 7).

Table 7: Pairwise comparison matrix created to establish factor weights for the criterion used to predict IOF runoff generating areas.

IOF	Pairwise Ranks			Individual Weights			Total Weights
	Porosity	NDVI	Land Use	Porosity	NDVI	Land Use	
Porosity	1.00	5.00	9.00	0.76271	0.78947	0.692308	0.748164414
NDVI	0.20	1.00	3.00	0.15254	0.15789	0.230769	0.180402113
Land Use	0.11	0.33	1.00	0.08475	0.05263	0.076923	0.071433473
SUM	1.31	6.33	13.00	1.00	1.00	1.00	1.00

3.4 MCE Algorithm

In this study, we used a Simple Additive Weighting approach to perform the MCE (Figure 6), where continuous criteria are rescaled to a standardized range (0-1) and combined using a weighted summation, shown in Equation 4 as:

$$\text{EQUATION 4: } \text{SUIT} = \sum w_k x_k$$

where SUIT is the suitability (index) layer resulting from the MCE (i.e., likelihood of runoff generation), and w_k are the various weights corresponding to each respective x_k layer (Bonnycastle *et al.*, 2017; Lamelas *et al.*, 2012).

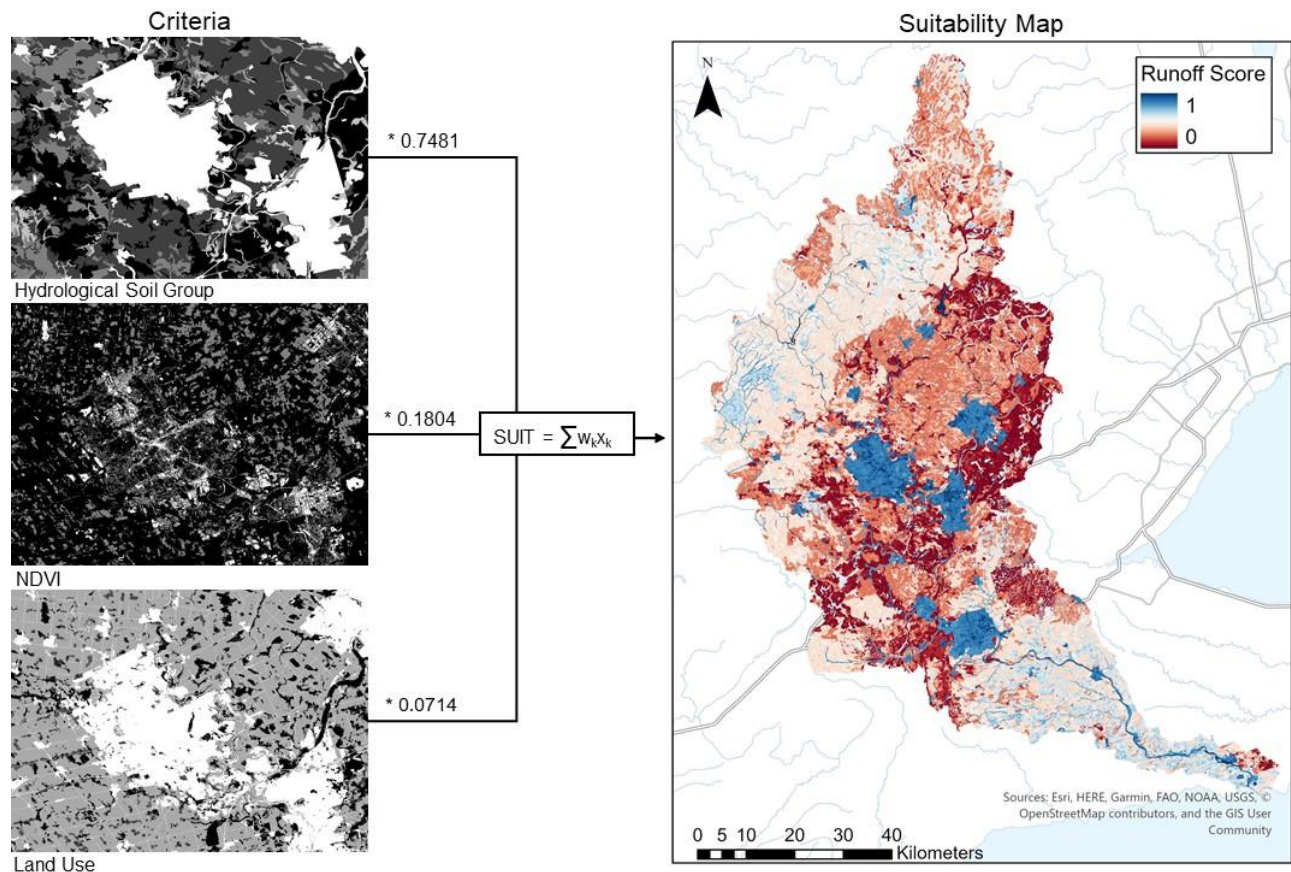


Figure 6: Image depicts the workflow for running the simple additive weighting MCE model. Each pre-processed criterion (left) is multiplied by its assigned weight, and all weighted layers are summed (i.e., overlaid) to produce a 'suitability' RGM index (i.e., runoff score). The output map is assigned values using the same scale as the input layers (0-1).

3.5 Linear Regression Analysis

Phosphorus data was retrieved from the Provincial (Stream) Water Quality Monitoring Network database. Quaternary watershed boundaries were retrieved from the Ontario Watershed Boundaries (OWB) collection released by the Provincial Mapping Unit (2020). Sub-watersheds that were located within the larger Grand River watershed were extracted from the provincial dataset. In total, 28 sub-watersheds lie within the Grand River watershed, and the IOF and SOF index maps were clipped to the boundaries of each of these sub-watersheds. Only stream monitoring stations at or near sub-watershed outlets were used in the regression analysis. A threshold distance of 5 km from sub-watershed outlets was used to select monitoring stations, assuming that water quality is relatively constant within a 5 km stream reach. Stations located downstream from major confluences with high order streams from other sub-watersheds were not included. This selection process was implemented to ensure phosphorus data was specific to its respective sub-watershed. Of the 28 sub-watersheds in the study area, 18 had monitoring stations which met the selection criteria and were used in the linear regression. All available phosphorus data from 2015 was averaged to yield an annual average phosphorus concentration for each monitoring station.

Index scores were calculated for each of the sub-watersheds by summing the index values for IOF and SOF independently in each of the sub-watersheds. Sums were then normalized by sub-watershed area to yield IOF and SOF normalized index scores. These scores are considered as an accurate quantification of the potential for both RGM in each of the 18 selected sub-watersheds. These scores were regressed with average phosphorus concentrations to evaluate their relationships.

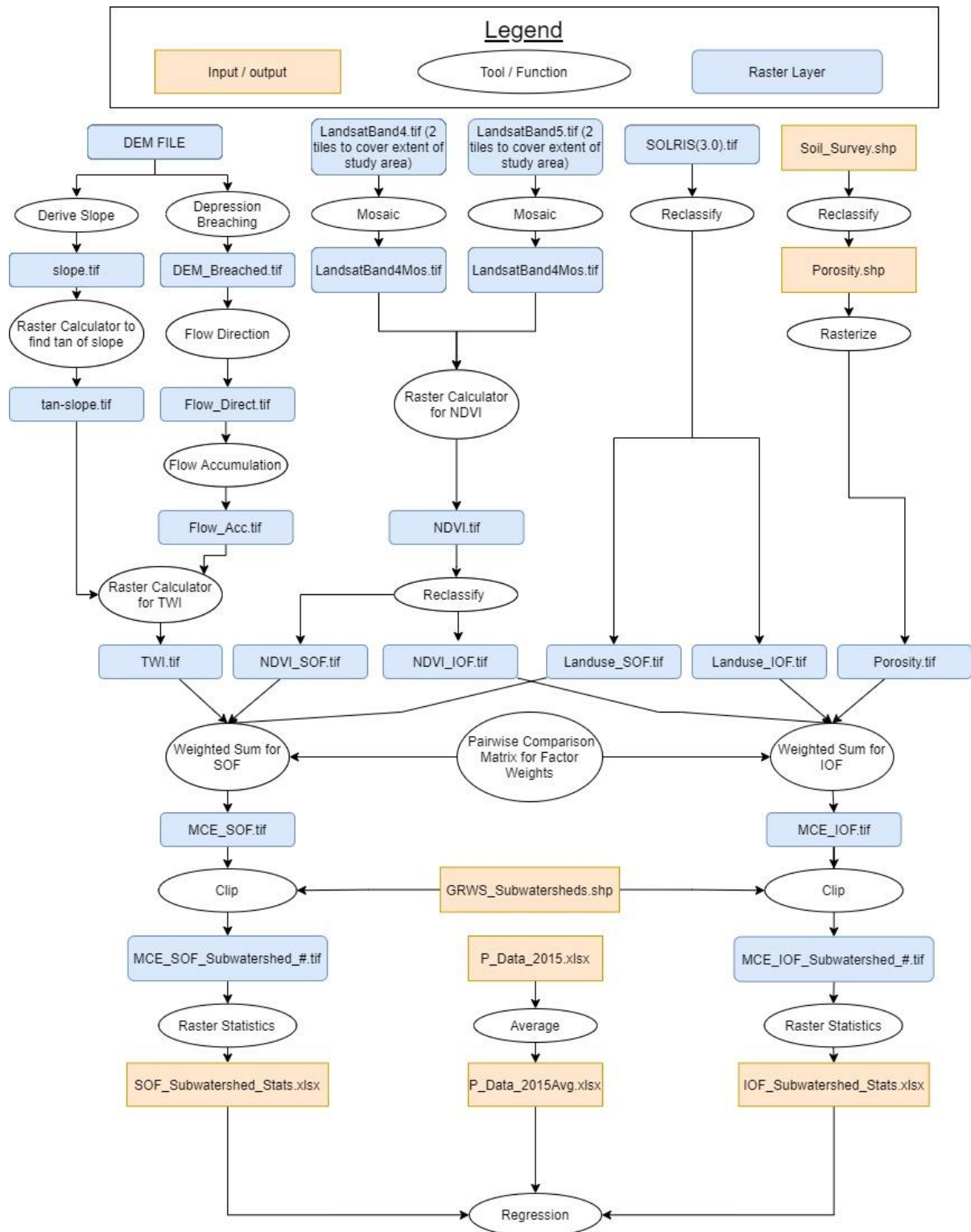


Figure 7: The project workflow for the development of various data layers, and how they were combined to perform the corresponding MCEs for SOF and IOF.

4. Results

4.1 Runoff Generation Indexes

The resulting IOF and SOF runoff generation indexes are presented in Figure 8. Visually, the resulting indexes look quite dissimilar in respect to the spatial distribution of HAAs across the landscape. Since the IOF criterion were rasterized from broad-scale discrete vector polygons, the model predicted that large areas (such as cities and agricultural fields) were likely to produce runoff. Opposingly, the SOF model results indicate that runoff only occurs in low-lying saturated areas, due in part to the use of continuous criteria (TWI). This coincides with previous research which found that IOF runoff occurs over larger areas, whereas SOF tends to be more localized and isolated to topographic depressions (Panjabi *et al.*, 2020).

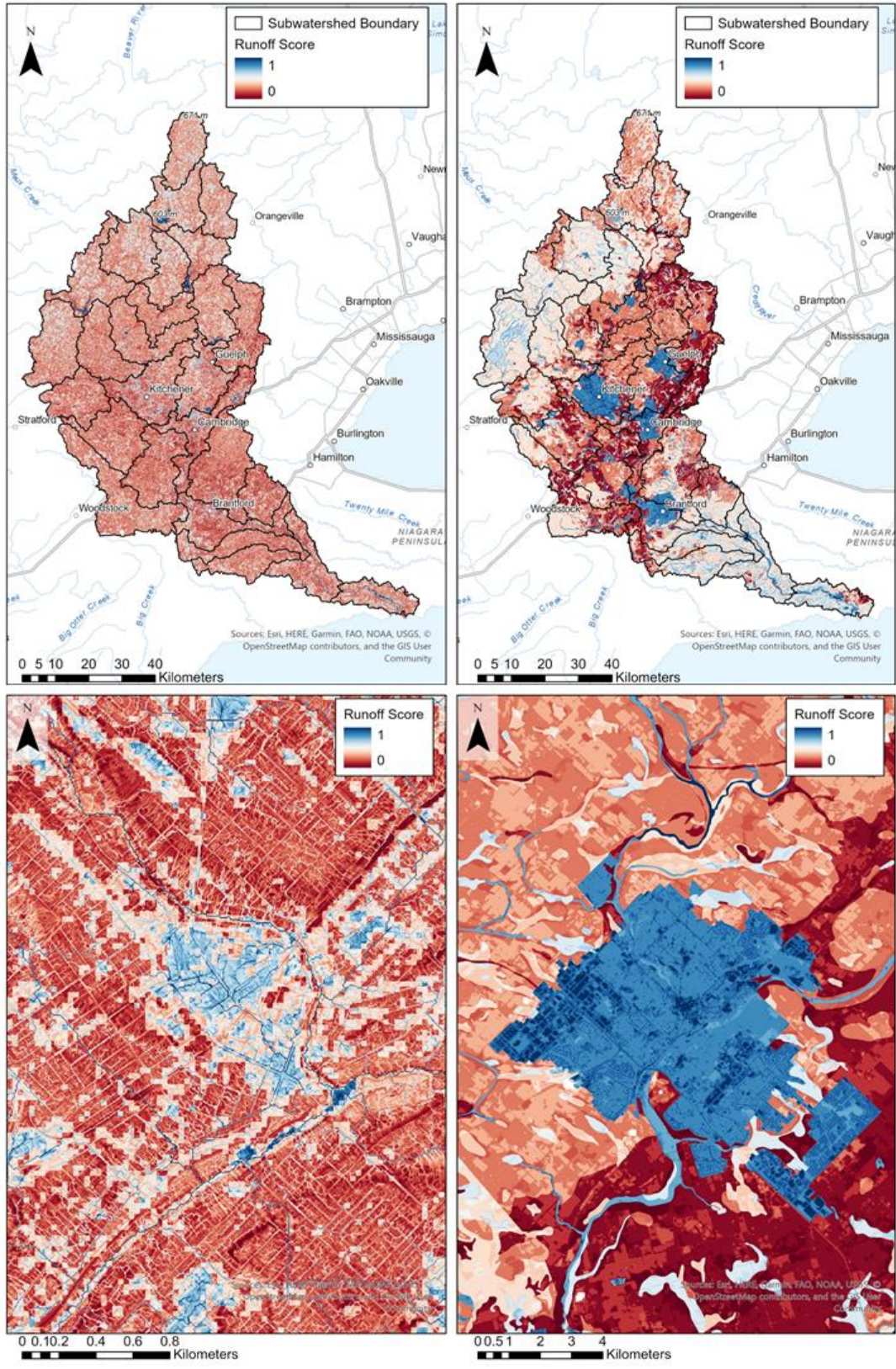


Figure 8: Runoff generation index maps after performing SAW process. The left maps (top and bottom) depict the results for probable SOF runoff generating areas, and the right maps (top and bottom) depict the results for IOF.

The finer scale images (bottom row), showing runoff scores for Guelph, ON, highlight the contrasting continuous and discrete nature of the MCE outputs for SOF and IOF respectively. Sub-watershed boundaries are also depicted in the maps in the top row, representing the 28 sub-watersheds used to clip the MCE output maps.

4.2 Relationships Between Normalized Runoff Generation Indexes and Average Phosphorus Concentrations at the Sub-Watershed Scale

Results from the linear regression returned diverging results for the two normalized RGM indexes. It was determined that the normalized IOF index is positively correlated with phosphorus concentrations as displayed by the positive coefficient in the regression equation ($y = 5.06E-06(x) - 0.01$; $R^2 = 0.312$; $p\text{-value} = 0.016$). The R-squared value indicates that the IOF index accounts for about a third of the variance in the phosphorus concentration data. The p-value indicates that this information can be accepted at greater than 98% confidence. In contrast, the normalized SOF index is negatively correlated with phosphorus concentrations as displayed by the negative coefficient in the regression equation ($y = -1.57E-05(x) + 0.19$; $R^2 = 0.087$; $p\text{-value} = 0.236$). The low R-squared value indicates that the SOF index is not well correlated with phosphorus concentrations. The high p-value indicates that this information is also likely not statistically significant. Based on the results from the linear regressions, the normalized IOF index is a better predictor for phosphorus concentrations than the SOF index.

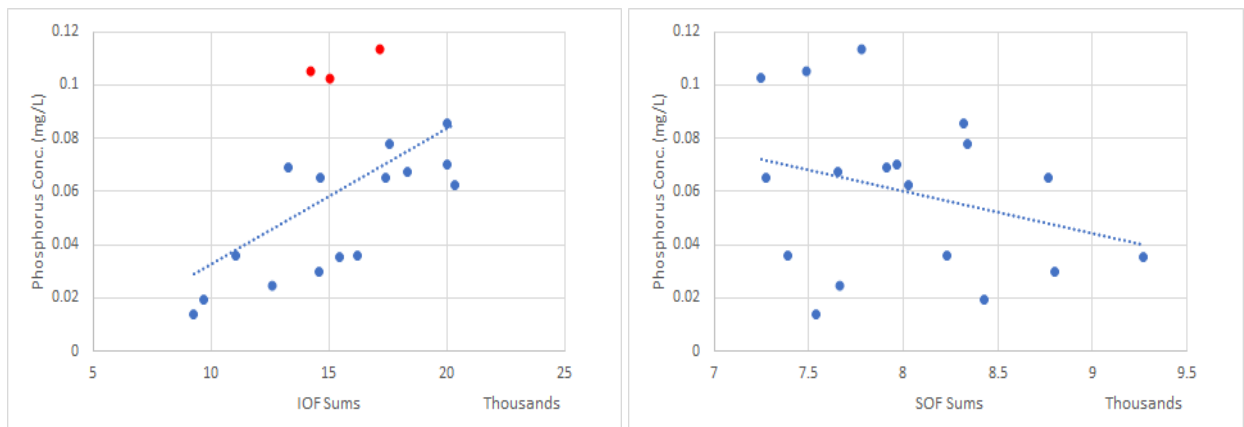


Figure 9: Scatter plots and regression lines from linear regression models for IOF index (left) and SOF index (right). Outlier points are indicated in red.

The three most significant outliers in the IOF regression (based on distance from the regression line; points highlighted in red in Figure 9) were investigated further using Google satellite imagery to see if their deviance could be explained by land cover characteristics. The three outlier points above the regression line had much higher phosphorus concentrations than expected compared to potential IOF runoff generation in their respective watersheds. All three stream monitoring locations are situated less than 3 km downstream of large urban centers (Brantford, Kitchener and New Hamburg) which are likely disproportionately increasing the concentrations of phosphorus near the outlets (Janke *et al.*, 2017). Results also indicate that SOF is less variable per watershed area compared to IOF, as displayed by the narrower boxplot range (Figure 10).

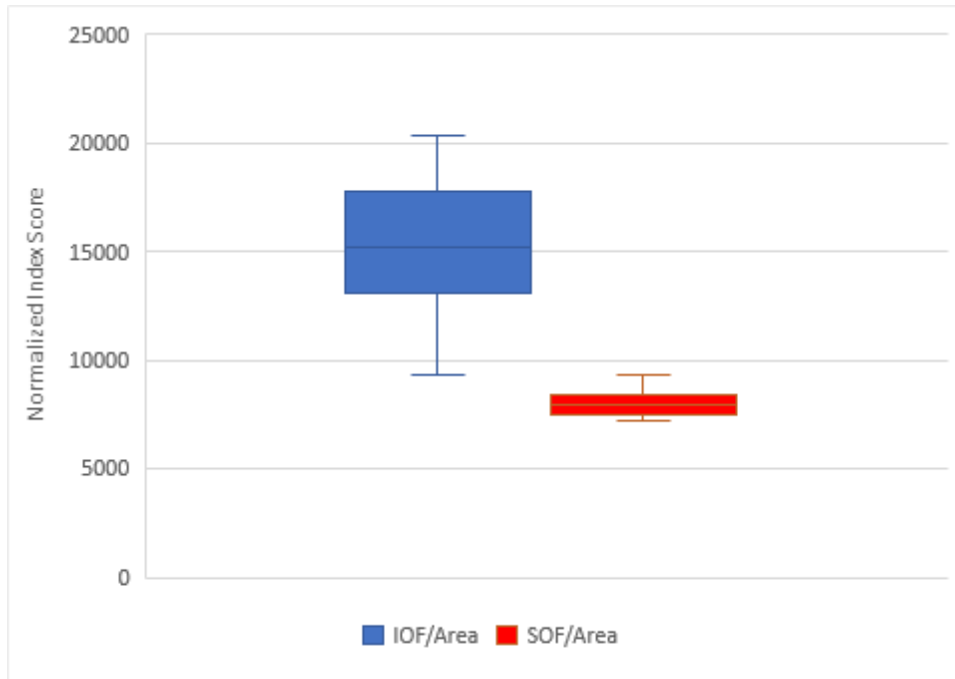


Figure 10: Box plots for normalized IOF and SOF index scores for the 18 sub-watersheds used in the linear regression. Boxes include median lines. Boxes represent the 2nd and 3rd quartiles for the normalized sub-watershed scores. Whiskers represent the 1st and 4th quartiles. N = 18.

5. Discussion

Modelling the spatial distribution of HAAs is challenging, as runoff generation is influenced by a broad range of variables. We considered the most important variables for each RGM, but additional variables such as hydrological conductivity of soils, underlying geology, antecedent conditions, and storm properties (i.e., intensity, duration) are more difficult to accurately represent (Panjabi *et al.*, 2020; Sen *et al.*, 2010). Despite these challenges, the models were able to identify distinct areas across the landscape where each RGM is most likely to occur based on variables considered. Because SOF is highly influenced by flow direction and flow accumulation, it modelled distinct flow pathways better than IOF did. While IOF was predicted to occur over broader areas, a limit to the IOF map is that it did not consider or model flow pathways.

The results from the linear regression indicate that IOF is the dominant RGM driving phosphorus transport from surface to stream, and that greater IOF runoff generation potential in watersheds equates to higher phosphorus concentrations in streams. Results also indicate that greater SOF potential may decrease phosphorus concentrations in associated streams. These results may be explained by specific RGM characteristics. IOF typically occurs in areas where water is more likely to be transported across a surface with elevated slope (Reli *et al.*, 2016). Oppositely SOF will typically extend outwards from areas of water accumulation and may eventually drain back into the depression it extended from (Thomas *et al.*, 2016). Accounting for flow pathways would improve the accuracy of the IOF index, so while this

relationship is not based upon a precise flow map, these results support that IOF is the larger driver of phosphorus from surface to stream.

In addition to spatial variability of runoff generating areas, it is also important to understand the hydrologic connectivity of these areas. Hydrologic connectivity refers to the water movement from one location to another on a landscape which can generate some surface runoff response (Bracken & Croke, 2007). While the SOF index accounts for hydrological connectivity and model flow pathways more accurately than IOF, it showed the lowest correlation with phosphorus. While the statistical relationship between IOF and phosphorus concentrations was stronger, the results indicate there are more complex mechanisms at play (i.e., phosphorus source zones and recharge times). Overall, the MCE approach to modelling surface runoff is a reasonable and manageable way of mapping HAAs and can be used in determining the dominant runoff generating mechanism in a watershed. This model provides interesting results given data limitations and can be reproduced easily in other watersheds with limited data and GIS-expertise.

6. Conclusion

This study presents a new method for quantifying runoff generation potential through SOF and IOF indexes and adds to our understanding of how surface hydrological processes impact phosphorus concentrations. The results indicate that IOF is more closely related with phosphorus transport, and this should be considered when planning targeted mitigation strategies to address phosphorus pollution. The results of this study should be used in conjunction with known phosphorus loading zones to quantify hydrologically sensitive areas (HSA), which consider surface runoff propensity, hydrological connectivity, and nutrient sources (Thomas *et al.*, 2016). These recommendations could be applied in future research to identify the most critical areas for nutrient loading mitigation with respect to runoff generation potential. Furthermore, to improve on the SOF and IOF results, future studies should consider additional variables for each RGM and could include flow maps to better quantify runoff reaching stream networks.

References

- Ali, G., & Creed, I. F. (2017b). Quantifying hydrologic connectivity of wetlands to surface water systems. *Hydrology and Earth System Sciences*, 21(3), 1791–1808.
<https://doi.org/10.5194/hess-21-1791-2017>
- Ali, G., Wilson, H., Elliott, J., Penner, A., Haque, A., Ross, C., & Rabie, M. (2017). Phosphorus export dynamics and hydrobiogeochemical controls across gradients of scale, topography and human impact. *Hydrological Processes*, 31(18), 3130–3145.
<https://doi.org/10.1002/hyp.11258>
- Brown, J. (n.d.). NDVI, the foundation for remote SENSING PHENOLOGY. Retrieved April 10, 2021, from https://www.usgs.gov/core-science-systems/eros/phenology/science/ndvi-foundation-remote-sensing-phenology?qt-science_center_objects=0#qt-science_center_objects
- Bonnycastle, A., Yang, W., & Mersey, J. (2017). *GEOG*3480 Manual: Introduction to Spatial Analyst in ArcGIS*. University of Guelph.
- Calhoun, A. J. K., Mushet, D. M., Alexander, L. C., DeKeyser, E. S., Fowler, L., Lane, C. R., Lang, M. W., Rains, M. C., Richter, S. C., & Walls, S. C. (2017). The Significant Surface-Water Connectivity of “Geographically Isolated Wetlands.” *Wetlands (Wilmington, N.C.)*, 37(4), 801–806. <https://doi.org/10.1007/s13157-017-0887-3>
- Chisholm, P.S., R. W. Irwin, and C. J. Acton, 1984. Interpretation of Soil Drainage Groups from Soil Taxonomy-Southern Ontario. *Can. J. Soil Science*. 64: 383-393.
- Endreny, T. A. (2005). Land use and land cover effects on runoff processes: Urban and suburban development. *Encyclopedia of Hydrological Sciences*. doi:10.1002/0470848944.hsa122
- Environment and Climate Change Canada (ECCC), 2018. Canada-Ontario Lake Erie Action Plan. Ontario, Canada. Report Number: En164-54/2018E-PDF
- Grand River Conservation Authority (GRCA). (2020). Our watershed.
<https://www.grandriver.ca/en/our-watershed/Our-Watershed.aspx>
- Grand River Information Network. (2018, October 30). Geospatial Data: Downloads. Retrieved March 6, 2021, from <https://data.grandriver.ca/downloads-geospatial.html>
- Gburek WJ, Sharpley AN. (1998). Hydrologic controls on phosphorus loss from upland agricultural watersheds. *Journal of Environmental Quality*, 2(7), 267–277.
<https://doi.org/10.2134/jeq1998.00472425002700020005x>
- Heathwaite, A. L., Quinn, P. F., & Hewett, C. J. M. (2005). Modelling and managing critical source areas of diffuse pollution from agricultural land using flow connectivity

- simulation. *Journal of Hydrology*, 304(1), 446–461.
<https://doi.org/https://doi.org/10.1016/j.jhydrol.2004.07.043>
- Helalia, A. M. (1993). The relation between soil infiltration and effective porosity in different soils. *Agricultural Water Management*, 24(1), 39–47. [https://doi.org/10.1016/0378-3774\(93\)90060-N](https://doi.org/10.1016/0378-3774(93)90060-N)
- Hoang, L., Schneiderman, E. M., Moore, K. E. B., Mukundan, R., Owens, E. M., & Steenhuis, T. S. (2017). Predicting saturation-excess runoff distribution with a lumped hillslope model: SWAT-HS. *Hydrological Processes*, 31(12), 2226–2243.
<https://doi.org/10.1002/hyp.11179>
- Janke, B. D., Finlay, J. C., & Hobbie, S. E. (2017). Trees and Streets as Drivers of Urban Stormwater Nutrient Pollution. *Environmental Science & Technology*, 51(17), 9569–9579. <https://doi.org/10.1021/acs.est.7b02225>
- Lamelas, M., Marinoni, O., Riva, J., & Hoppe, A. (2012). Comparison of multi-criteria analysis techniques for environmental decision making on industrial location. In C. Jao (Ed.), *Decision support systems* (pp. 197–221)
- Lindsay, J. (2018). Whitebox Tools User Manual: Image Processing Tools.
https://jblindsay.github.io/wbt_book/available_tools/image_processing_tools_image_enhancement.html#GaussianContrastStretch
- Lindsay, J. (2020). Whitebox Tools User Manual: Hydrological Analysis.
https://jblindsay.github.io/wbt_book/available_tools/image_processing_tools_image_enhancement.html#GaussianContrastStretch
- Liu, Y., Yang, W., Leon, L., Wong, I., McCrimmon, C., Dove, A., & Fong, P. (2016). Hydrologic modeling and evaluation of Best Management Practice scenarios for the Grand River watershed in Southern Ontario. *Journal of Great Lakes Research*, 42(6), 1289–1301.
<https://doi.org/10.1016/j.jglr.2016.02.008>
- Liu, Y., Zhang, K., Li, Z., Liu, Z., Wang, J., & Huang, P. (2020). A hybrid RUNOFF generation modelling framework based on SPATIAL combination of three RUNOFF generation schemes FOR semi-humid and SEMI-ARID WATERSHEDS. *Journal of Hydrology*, 590, 125440. doi:10.1016/j.jhydrol.2020.125440
- Molder, B., Cockburn, J., Berg, A., Lindsay, J., & Woodrow, K. (2015). Sediment-assisted nutrient transfer from a small, no-till, tile drained watershed in Southwestern Ontario, Canada. *Agricultural Water Management*, 152, 31–40.
<https://doi.org/10.1016/j.agwat.2014.12.010>

- Niehoff, D., Fritsch, U., & Bronstert, A. (2002). Land-use impacts on storm-runoff Generation: Scenarios of LAND-USE change and simulation of hydrological response in A Meso-scale catchment in SW-Germany. *Journal of Hydrology*, 267(1-2), 80-93. doi:10.1016/s0022-1694(02)00142-7
- Ontario Provincial Mapping Unit – Mapping and Resources Information Branch. Ontario Watershed Boundaries (OWB) collection. 2020. Metadata identifier: 53a1c537b320404087c54ef09700a7db
- Outram, F. N., Cooper, R. J., Sünnerberg, G., Hiscock, K. M., & Lovett, A. A. (2016). Antecedent conditions, hydrological connectivity and anthropogenic inputs: Factors affecting nitrate and phosphorus transfers to agricultural headwater streams. *Science of The Total Environment*, 545–546, 184–199. <https://doi.org/https://doi.org/10.1016/j.scitotenv.2015.12.025>
- Panjabi, K., Rudra, R., Goel, P., Daggupati, P., Shrestha, N. K., Shukla, R., Zhang, B., & Allataifeh, N. (2020). Mapping runoff generating areas using AGNPS-VSA model. *Hydrological Sciences Journal*, 65(13), 2224–2232. <https://doi.org/10.1080/02626667.2020.1798007>
- Raduła, M. W., Szymura, T. H., & Szymura, M. (2018). Topographic wetness index explains soil moisture better than bioindication with Ellenberg's indicator values. *Ecological Indicators*, 85, 172–179. <https://doi.org/10.1016/j.ecolind.2017.10.011>
- Reli, S., Mohamad Yusoff, I., Lateh, H., & Ujang, U. (2016). A Review of Infiltration Excess Overland Flow (IEOF): Terms, Models and Environmental Impact. *JOURNAL OF ADVANCES IN HUMANITIES*, 4, 490–502. <https://doi.org/10.24297/jah.v4i2.5098>
- Saaty, T. (1977). A scaling method for priorities in hierarchical structures. *Journal of Mathematical Psychology*, 15(3), 234-281. [https://doi.org/10.1016/0022-2496\(77\)90033-5](https://doi.org/10.1016/0022-2496(77)90033-5)
- Sen, S., Srivastava, P., Dane, J. H., Yoo, K. H., & Shaw, J. N. (2010). Spatial–temporal variability and hydrologic connectivity of runoff generation areas in a North Alabama pasture—implications for phosphorus transport. *Hydrological Processes*, 24(3), 342–356. <https://doi.org/10.1002/hyp.7502>
- Srinivasan, M.S., Gburek, W.J., & Hamlett, J.M. (2002). Dynamics of stormflow generation—a hillslope-scale field study in east central Pennsylvania, USA. *Hydrological Processes*, 16, 649–665. <https://doi.org/10.1002/hyp.311>
- Thomas, I. A., Jordan, P., Mellander, P.-E., Fenton, O., Shine, O., Ó hUallacháin, D., Creamer, R., McDonald, N. T., Dunlop, P., & Murphy, P. N. C. (2016). Improving the identification of hydrologically sensitive areas using LiDAR DEMs for the delineation and mitigation of

critical source areas of diffuse pollution. *The Science of the Total Environment*, 556, 276–290. <https://doi.org/10.1016/j.scitotenv.2016.02.183>

USGS - U.S. Geological Survey. (2020, September 8). EarthExplorer2. Retrieved March 2, 2021, from <https://earthexplorer.usgs.gov/>

Wu, Q., & Lane, C. R. (2017). Delineating wetland catchments and modeling hydrologic connectivity using lidar data and aerial imagery. *Hydrology and Earth System Sciences*, 21(7), 3579–3595. <https://doi.org/10.5194/hess-21-3579-2017>

Zimmermann, B., Elsenbeer, H., & De Moraes, J. M. (2006). The influence of land-use changes on soil hydraulic properties: Implications for runoff generation. *Forest Ecology and Management*, 222(1-3), 29-38. doi:10.1016/j.foreco.2005.10.070

Zollweg, J.A., Gburek, W.J., Pionke, H.B., & Sharpley, A.N. (1995). GIS-based delineation of source areas of phosphorus within agricultural watersheds of the northeastern USA. Proceedings of the IAHS Symposium on Modeling and Management of Sustainable Basinscale Water Resources Systems, 10–14 July, Boulder, Colorado, 31–39. <https://www.researchgate.net/publication/40190251> [Analysis of regional water resources and their management by means of numerical simulation models and satellites in Mendoza Argentina](https://www.researchgate.net/publication/40190251)

